Physical properties of quasi-one-dimensional $SrNbO_{3.41}$ and Luttinger liquid analysis of electrical transport

A. de Campos,[1,*] M. S. da Luz,[1,*] C. A. M. dos Santos,[1,2] A. T. Rice,[1] A. M. Deml,[1] B. D. White,[1] J. J. Neumeier,[1] and J. L. Cohn[3]

[1]*Department of Physics, Montana State University, P.O. Box 173840, Bozeman, Montana 59717-3840, USA*

[2]*Escola de Engenharia de Lorena-USP, P.O. Box 116, Lorena 12602-810, SP, Brazil*

[3]*Department of Physics, University of Miami, Coral Gables, Florida 33124, USA*

(Received 15 June 2010; revised manuscript received 18 August 2010; published 20 September 2010)

We report the diagonal components of the electrical resistivity tensor of quasi-one-dimensional $SrNbO_{3.41}$, determined using the Montgomery method. The results confirm quasi-one-dimensional behavior but show a smaller anisotropy than previously reported. High-resolution linear thermal expansion reveals weakly anisotropic behavior and no evidence of charge-density wave formation, which has been suspected as the cause of the upturn in the electrical resistivity ρ near 50 K. Heat-capacity measurements reveal an electronic heat-capacity coefficient that is near zero with a Debye temperature $\Theta_D=382(1)$ K. We report that ρ exhibits power-law behavior, as expected within the framework of Luttinger liquid theory for quasi-one-dimensional systems. Detailed analysis of the data above 100 K implies relatively strong correlations and the possibility of a gap in the spin-excitation spectrum. The origin of the small energy gap below 50 K and the conduction mechanism in this region remain as outstanding issues.

DOI: 10.1103/PhysRevB.82.125117 PACS number(s): 71.10.Pm, 72.80.−r, 65.40.De, 65.40.Ba

I. INTRODUCTION

The family of quasi-one-dimensional (1D) materials belonging to the homologous series $A_nB_nO_{3n+2}$ differs slightly from the three-dimensional network of the ABO_3 perovskite structure by the presence of excess oxygen.[1] The $SrNbO_{3.5-x}$ system, in particular, has unusual chemical and physical properties. Depending on the oxygen stoichiometry, these niobium oxides exhibit highly anisotropic electrical transport ($SrNbO_{3.41}$) or ferroelectricity ($SrNbO_{3.5}$) with a very high transition temperature.[1] $SrNbO_{3.41}$ has an orthorhombic symmetry (*Pnnm*) with lattice parameters[2,3] $a=3.995$ Å, $b=5.674$ Å, and $c=32.456$ Å. Electrical transport, angle-resolved photoemission, infrared spectroscopy, and band-structure calculations all agree that it is a quasi-one-dimensional material.[1,4–6]

The temperature dependence of the electrical resistivity along the a axis, ρ_a, can be divided into several pertinent regimes. Note that we refer to the crystallographic directions[3] according to the convention adopted in other work that reported on anisotropy in physical properties,[1,4–6] where the a axis has the lowest electrical resistivity. Upon cooling, $\rho_a(T)$ increases weakly until roughly 125 K after which it decreases followed by another increase starting near 50 K.[1,4] Similar temperature dependence is observed for $\rho_b(T)$ although the decrease below 125 K is less pronounced. Along the c axis, there is only an inflection point near 125 K and then $\rho_c(T)$ increases upon cooling over the entire temperature range. The highest electrical conductivity occurs along a and an anisotropic resistivity ratio[1] at 300 K of $\rho_a:\rho_b:\rho_c \sim 1:10^2:10^4$ was observed. There is some uncertainty as to the source for the upturn in $\rho(T)$ below 50 K, which corresponds to an energy gap of a few millielectron volts.[1,4,5] The possibilities of a gapped charge-density wave (CDW) or the opening of a Mott-Hubbard gap have been discussed,[1,4] although neither of these seem to be fully accepted.

Previous $\rho(T)$ measurements were conducted using a standard four-contact method. It is well known that this intermixes conductivity contributions from all three axes, even if the current is applied along one principal crystallographic axis. Elimination of these contributions requires use of a method such as that of Montgomery,[7,8] which determines the diagonal components of the electrical resistivity tensor. This method is applied herein to provide a better assessment of the low-dimensional electrical conduction. We also report measurements of high-resolution thermal expansion using a thermal expansion cell constructed of fused quartz, which can detect 0.1 Å changes in specimen length for a relative resolution[9] of about 10^{-8}. This resolution is more than sufficient to reveal structural changes associated with electronic phase transitions, such as the formation of a CDW.[10,11] In addition, we report measurements of heat capacity in the temperature range $0.3\ \text{K} < T < 300$ K. The results reveal that the existence of a CDW in $SrNbO_{3.41}$ is highly unlikely. Further analysis of the electrical resistivity reveals power-law behavior that is consistent with quasi-one-dimensional electrical transport. This observation is discussed within the framework of theories for Luttinger liquids (LLs), which reveals that the data above 80 K imply relatively strong correlations and the possibility of a gap in the spin-excitation spectrum. Below 50 K the behavior of ρ and the origin of the small gap[5] remain unclear; some possibilities are discussed.

II. EXPERIMENTAL

Single crystals of $SrNbO_{3.41}$ were grown by the optical-floating-zone (OFZ) technique.[1] The synthesis involved the following steps. First, $SrCO_3$ (99.99%, Alfa) and Nb_2O_5 (99.9%, Alfa) powders were weighed and mixed in an agate mortar followed by reacting and heating for 6 h at 1250 °C in air to yield $SrNb_{0.964}O_{3.41}$. Care was taken to keep the powders as moisture free as possible. The carbonate was

heated for several hours, then stored in a dry atmosphere. The $SrNb_{0.964}O_{3.41}$ sample was reground and pressed into cylindrical rods by packing the powder into latex tubes followed by compaction with hydrostatic pressure. The polycrystalline rods were sintered at 1400 °C for 6 h under a mixed atmosphere of 3% hydrogen and 97% argon. Finally, $SrNbO_{3.41}$ single crystals were grown in an OFZ furnace (NEC model SCI-MDH-20020) in the previously mentioned atmosphere flowing at 1.2 l/min through the growth chamber. The rotation rate of both polycrystalline rods was 5 rpm. That rate provided a stable, homogenous molten zone and advantageous liquid-solid interface. A growth rate of 7.5 mm/h for the upper rod and 5 mm/h for the lower rod was adopted. The lamp power in our two-lamp furnace was kept near 570 W (using 1000 W lamps) during the growth.

The layered structure of $SrNbO_{3.41}$ allowed the as-grown cylindrical boule to easily cleave along the *a*-*b* plane. The obtained crystal exhibited a flat surface with dimensions $16.0\times6.0\times1.0$ mm^3 which was cleaved and polished to different sizes for thermal-expansion, electrical-resistance, and heat-capacity measurements.

The single-phase nature of the crystals was determined by x-ray powder diffraction (Cu $K\alpha$ radiation). Two crystals were oriented using backreflection Laue x-ray diffraction and carefully polished in order to obtain rectangular shapes for better determination of the geometric factors. Electrical resistance was determined using the Montgomery method[7,8] with low-resistance vapor-deposited gold contacts, which were found to provide the most reliable, noise-free measurement data. We also measured the electrical resistivity using the standard four-probe method, whereby two samples were polished in the shape of long bars with a typical size of $3.0\times1.0\times0.2$ mm^3 and the long axis along either *a* or *b*. Montgomery[7,8] and four-probe dc electrical-resistance measurements were performed in the range $2<T<300$ K using a Quantum Design physical property measurement system (PPMS). We report the average of three measurements in each direction and the corresponding uncertainties. The crystal used for thermal expansion measurements had dimensions of $4.914\times1.966\times0.983$ mm^3 (*a*, *b*, and *c* axes, respectively). The data were collected at intervals ranging from 0.1 to 0.2 K using a warming rate of 0.20(1) K/min. The data are corrected for the empty-cell effect, measured in a separate experiment, and for the differential expansion between the cell and sample.[9] Heat capacity was measured using the PPMS, which utilizes a relaxation method.

III. RESULTS AND DISCUSSION

X-ray powder diffractometry, carried out with ground single crystals, showed only Bragg reflections from the orthorhombic structure of $SrNbO_{3.41}$ as described in previous work (see Fig. 1).[1,2] The crystal structure of $SrNbO_{3.41}$ is displayed in Fig. 1. It is built from NbO_6 octahedra blocks grouped into slabs that are five octahedra wide, which extend along the *c* direction. Only along the *a* axis are the octahedra connected in a continuous manner via their apical oxygen atoms, forming 1D chains.[1]

Figure 2 shows the electrical resistance as a function of temperature $R(T)$ for the three principal crystallographic directions using a geometry suitable for calculation of the electrical resistivity with the Montgomery method.[7,8] These data are shown for comparison to previously published data[1,4,13] since they illustrate the general temperature dependence prior to our computation of the tensor components of $\rho(T)$. The temperature dependencies are similar for all crystals measured in this work. Using the data in Fig. 2 and the Montgomery method, we calculated the diagonal components of the electrical resistivity tensor (ρ_{aa}, ρ_{bb}, and ρ_{cc}) as a function of temperature. The results are plotted in Fig. 3(a). The tensor components at 300 K are $\rho_{aa}(300\ \mathrm{K})=0.92(2)$ mΩ cm, $\rho_{bb}(300\ \mathrm{K})=33.82(5)$ mΩ cm, and $\rho_{cc}(300\ \mathrm{K})=779.3(4)$ mΩ cm. The uncertainties were calculated based on the uncertainties of the geometric factors.

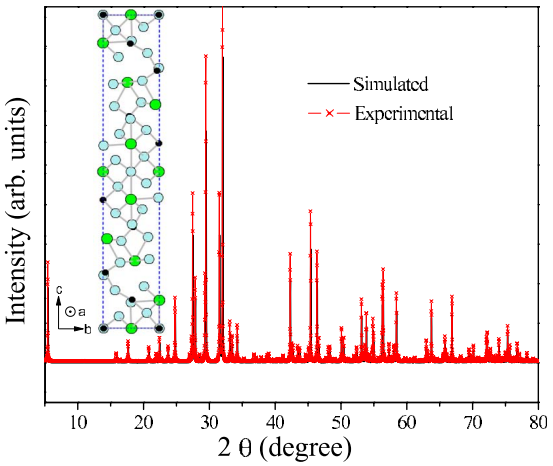

FIG. 1. (Color online) Experimental x-ray powder diffraction data for $SrNbO_{3.41}$ (red crosses) and simulation calculated with powder cell (Ref. 12). All Bragg reflections correspond to the expected pattern for $SrNbO_{3.41}$, as reported by Abrahams *et al.* (black line) (Ref. 2). The crystal structure is shown, projected on the (100) plane, with Nb denoted by black, Sr by green, and oxygen by blue circles.

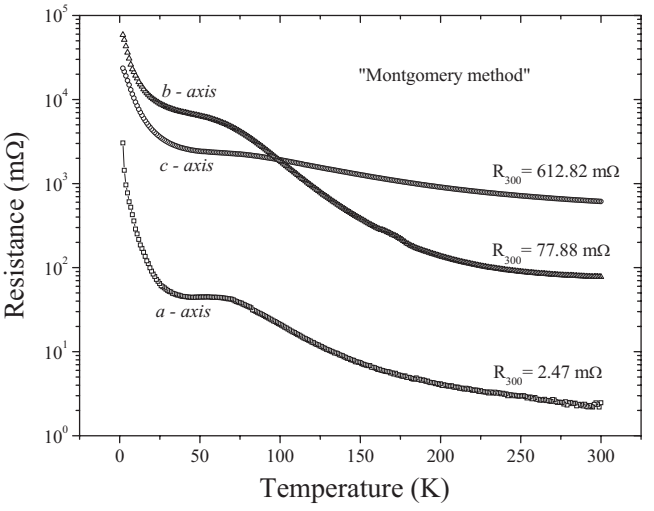

FIG. 2. Electrical resistance for the three principal crystallographic directions of a $SrNbO_{3.41}$ single crystal. The R_{300} values indicate the resistance at 300 K for each axis.

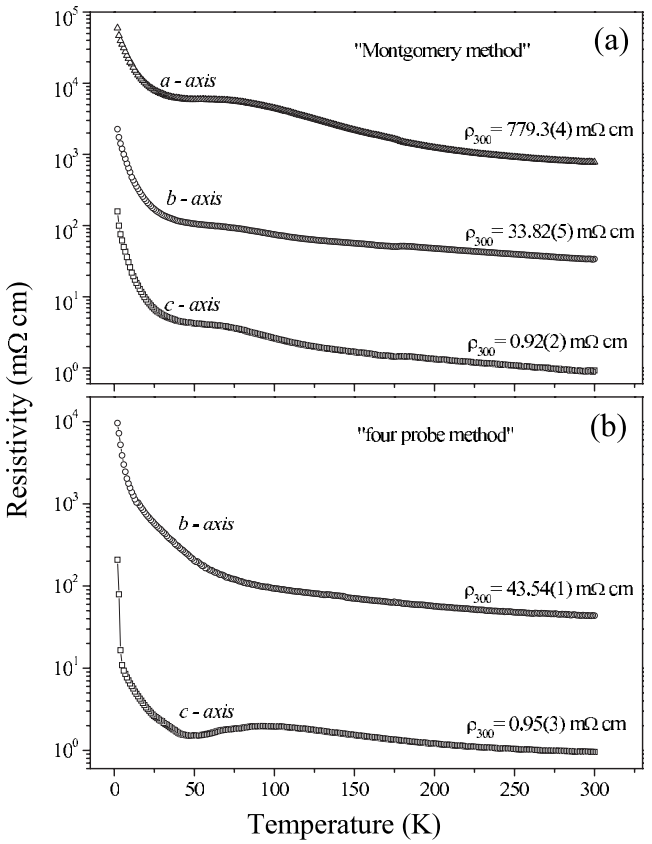

FIG. 3. (a) Electrical resistivity as a function of temperature for the three principal crystallographic directions of $SrNbO_{3.41}$ using the modified Montgomery method. The ρ_{300} values indicate the resistivity at 300 K for each axis. (b) Electrical resistivity as a function of temperature along the c and b axes as calculated using the standard four-probe method.

The tensor components at 300 K for a and b are larger by a factor of 2 and ~1.2, respectively, when compared to the ρ values reported previously.[1,4] (ρ_a=0.46 mΩ cm and ρ_b ~29 mΩ cm). On the other hand, the c-axis resistivity ρ_{cc}(300 K) is smaller by a factor of 1.5 from previous reports[1,4] (ρ_c ~1.2 Ω cm). The resistivity is still highly anisotropic with very low, metal-like values along the a direction. At 300 K, the anisotropy can be estimated by a ratio of $\rho_{aa}:\rho_{bb}:\rho_{cc}\sim 1:37:847$. The difference between these values and those reported previously[4] can be attributed to use of the conventional four-probe method, which intermixes contributions to ρ from all crystallographic directions and does not determine the diagonal components of the electrical resistivity tensor. A fit to the equation $\rho\sim\exp(E_a/k_BT)$ for the temperature range 20–40 K reveals an energy gap E_a ≈2.3 meV; this value is similar to that reported previously.[4]

To cross-check the values determined above, two long bars were cut and polished with the long axis along the a and b axes, respectively. We then measured $\rho(T)$ along these axes using the standard four-probe technique. These results are shown in Fig. 3(b). Resistivities at 300 K for a and b are ρ_a=0.95(3) mΩ cm and ρ_b=43.54(1) mΩ cm, respectively. This provides an anisotropic ratio of $\rho_a:\rho_b\sim 1:46$ which is comparable with the ratio obtained through the Montgomery method. This process was impossible for the c axis because cleaving of the samples did not allow fabrication of a bar with its long axis along c. Uncertainties in this method were estimated by comparing the size of the voltage contacts (0.1 mm) with the distance between them (~0.2 mm). Although these values possess large uncertainties, they provide confidence that the electrical resistivities determined by the Montgomery method are reliable.[7,8]

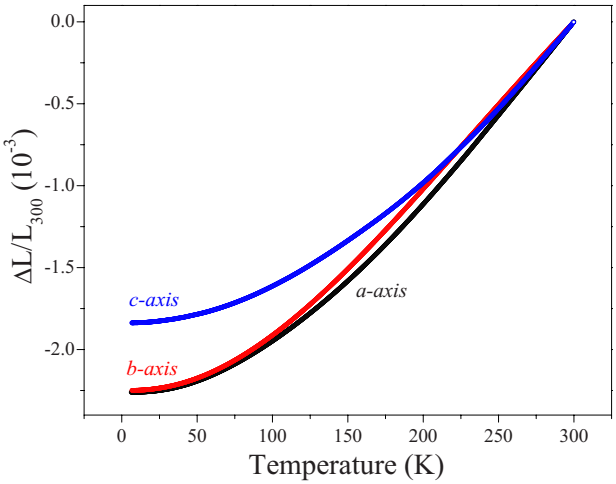

FIG. 4. (Color online) Linear thermal expansion ($\Delta L/L_{300}$) for the three principal crystallographic directions.

In order to further evaluate the low-dimensional nature of this material and to search for the origin of the upturn in $\rho(T)$, we measured the thermal expansion. The technique used in this work has a *relative* resolution of about 1 part in 10^8, which is at least 1000 times more sensitive than that possible with diffraction techniques.[9] Linear thermal expansion (LTE) normalized to the length at 300 K, $\Delta L/L_{300}$, is displayed in Fig. 4 for the a, b, and c axes of $SrNbO_{3.41}$. These are raw data, corrected only for the thermal expansion of quartz with no further processing.[9] The results reveal weakly anisotropic behavior. In spite of possible small variations in composition, the same behavior is observed for another crystal indicating good reproducibility. The overall (i.e., from 5 to 300 K) in-plane linear thermal expansions (a and b axes) are about 1.2 times larger in magnitude than that of the c axis. The LTE contracts along all three axes from room temperature to ~5 K with no obvious features in the $\Delta L/L_{300}$ data that might correspond to a phase transition, such as CDW formation. If a phase transition to a CDW state did occur, a change in slope of $\Delta L/L_{300}$ would be expected. This possibility is evaluated in more detail below when the thermal expansion coefficient is discussed.

Most notable is the fact that the observed behavior differs significantly from other layered oxides such as η-Mo_4O_{11}, γ-Mo_4O_{11}, $Li_{0.9}Mo_6O_{17}$, and $CaMn_2O_4$ where $\Delta L/L_{300}$ reveals strongly anisotropic behavior and, in some cases, shows negative thermal expansion along one or two crystallographic directions.[11,14–16] The general magnitude of $\Delta L/L_{300}$ and the thermal-expansion coefficient $\mu = d(\Delta L/L_{300})/dT$ (see Fig. 5) for the range 5–300 K (~2.5 $\times 10^{-3}$), is fairly comparable to other oxides,[17,18] such as $La_{0.7}Ca_{0.3}MnO_3$ and $YBa_2Cu_3O_7$. Transition-metal oxides typically have smaller thermal expansion than metallic ele-

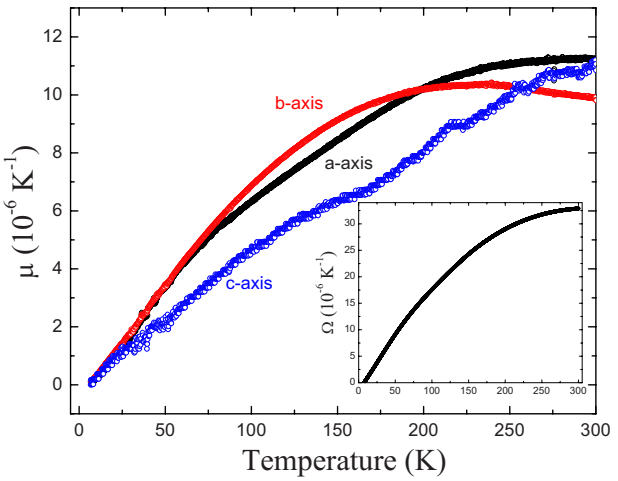

FIG. 5. (Color online) Thermal-expansion coefficient $\mu = (1/L_{300\ \mathrm{K}})d\Delta L/dT$ for the three principal crystallographic directions. In the inset, the volumetric thermal-expansion coefficient (Ω) versus T is shown.

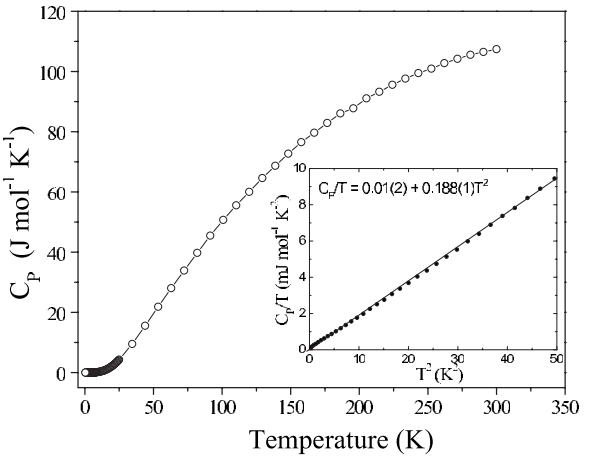

FIG. 6. Molar heat capacity C_P versus temperature; the line is a guide to the eyes. The inset shows C_P/T versus T^2 along with the linear fit.

ments such as copper and aluminum, which exhibit changes in $\Delta L/L_{300}$ of 3.2×10^{-3} and 4.1×10^{-3} over the same temperature range, respectively.[19]

Figure 5 displays the linear thermal-expansion coefficients, $\mu_i = d(\Delta L/L_{300})/dT$ for the $i=a$, b, and c axes. We determined μ_i using a point-by-point derivative of the data in Fig. 4. No data smoothing was conducted. When we examine μ_i, there are no indications of any features which might correspond to the inflection points observed in $\rho(T)$ below $\sim$80 K. There is significantly more scatter in the μ_c data. We believe that this is due to two issues: (1) the crystals are at least 50% thinner along this measurement direction and (2) the crystals have a natural tendency to cleave in thin layers perpendicular to this direction, which results in poor mechanical stability. Note that the scatter in μ_i near 45 K is an experimental artifact associated with our control of the warming rate of the thermal expansion cell. In the inset, the volumetric thermal-expansion coefficient $\Omega = \mu_a + \mu_b + \mu_c$ is displayed. These data were determined by fitting the μ_i data using Chebyshev polynomials[9] to generate μ_a, μ_b, and μ_c data with identical temperature values prior to adding the three data sets. The Ω data reveal no inflection points that might correspond to CDW behavior.

The behavior in the data of Fig. 5 differ markedly from what is typically observed in phonon-induced (CDW) systems such as γ-Mo_4O_{11} (Ref. 11) and $K_{0.3}MoO_3$,[10] where appreciable jumps in μ_i and Ω clearly indicate a thermodynamic phase transition associated with CDW formation. The absence of such features lead us to conclude that the upturn in $\rho(T)$ below $T\sim50$ K is not the result of a CDW.

The molar heat capacity C_P as a function of temperature is displayed in Fig. 6 for 0.3 K$<T<$300 K. C_P is smooth and well behaved over the entire temperature range with no features that might indicate the presence of a phase transition. At low temperature, a plot of C_P/T versus T^2 allows comparison to the expected behavior $C_P/T = \gamma + \beta T^2$. When plotted in this manner, the data exhibit linear behavior in the range $0.1<T^2<50$ K^2 with an intercept of $\gamma\approx0$ (fit parameters appear in inset of Fig. 6). The fit reveals a value of $\beta = 0.188(1)$ mJ mol^{-1} K^{-4}, which leads to a Debye temperature of $\Theta_D = 382(1)$ K. The C_P/T versus T^2 data appear to show a slight upturn on cooling below $T^2<20$ K. We fit this region and found a value of $\gamma = 0.079(8)$ mJ mol^{-1} K^{-2}, which we take as the upper limit. Theory for one-dimensional Fermi systems exhibiting Luttinger liquid behavior predicts a linear term in the heat capacity.[20] Thus, our results are not in disagreement with this possibility but the small value of γ suggests localized electrons or a small density of states at the Fermi energy.

Having established, within the sensitivity of our measurements, that the upturn in $\rho(T)$ below $T\sim50$ K is not associated with a CDW transition, we conduct some further analysis of the electrical resistivity. Figure 7(a) displays the data of Fig. 3(a) plotted on a log-log scale. Immediately apparent for the a and b data are two fairly linear regions above and below the temperature range where the upturn in $\rho(T)$ occurs, indicative of power-law behavior. In contrast, the c axis is not linear above the upturn. This behavior is clarified in the log $\rho(T)$ versus $1/T$ plot in Fig. 7(b), which reveals the high-temperature region of ρ_{cc} (see inset) to be activated with an energy gap $E_a\approx28$ meV ($E_a/k_B\approx325$ K).

The apparent power-law behavior together with the documented quasi-one-dimensional electrical conductivity lead us to an interpretation based on the theory for LLs.[20] Though an approximate power-law behavior in $\rho(T)$ is also evident for the low-T regime, 6 K$\leq T\leq$20 K [Fig. 7(a)], LL physics would appear to be inapplicable given other evidence (optical and photoemission)[4] for the opening of a small energy gap at $T\leq50$ K. Non-Fermi liquid behavior in such systems is most likely to be manifested at high temperatures, beyond possible temperature scales for a Mott-Hubbard gap[20] or dimensional crossover,[21] thus we focus on the power-law behavior of the data at $T\gtrsim80$ K (see Fig. 8). To our knowledge the resistivity of $SrNbO_{3.41}$ in this regime has not previously been examined in this context.

Along the conducting chains, theory[20,21] predicts $\rho_\parallel \propto T^\beta$, with[22] $\beta = n_c^2K_c + n_s^2K_s - 3$. Here K_c and K_s are LL parameters in the charge and spin sectors, respectively ($K_c=1$ corre-

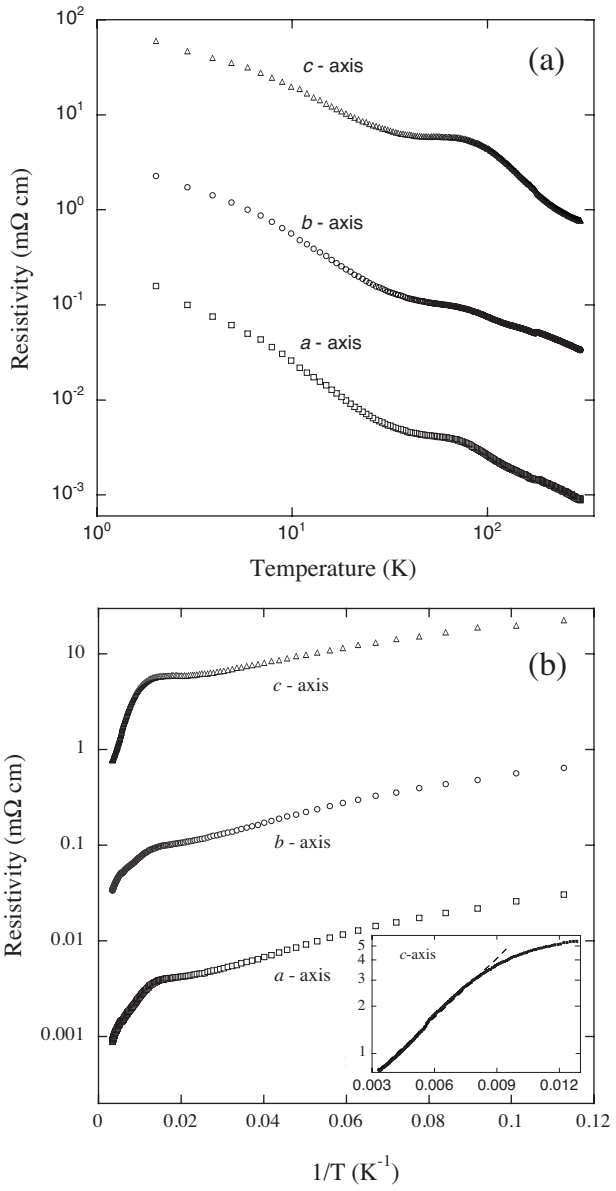

FIG. 7. (a) Electrical resistivity versus temperature plotted on a log-log scale. (b) Same data shown on a log versus $1/T$ scale. Inset displays the linear region for the c-axis data in the range 120 K $<T<300$ K. Dashed line is a guide to the eyes.

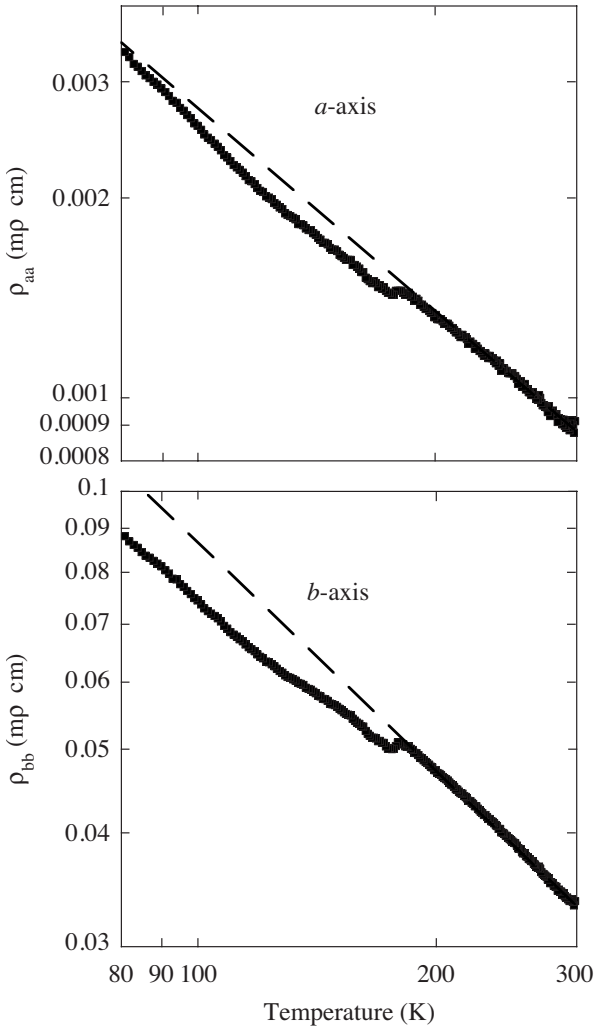

FIG. 8. Electrical resistivity versus temperature plotted on a log-log scale for the a axis (top panel) and the b axis (lower panel). The dashed lines are a guide to the eyes. Neglecting the slight jump (Ref. 23) in the a-axis data, the region of linearity extends to nearly 100 K. Along the perpendicular direction (i.e., the b axis), the region of linearity is smaller, extending to about 150 K.

sponds to noninteracting electrons), n_c is the order of commensurability, and $n_s=0(1)$ for even (odd) commensurability. The commensurability is determined by the ratio of the Fermi momentum to the size of the Brillouin zone, i.e., $k_F a=\pi/n_c$ with $n_c=2$, 3, and 4 corresponding to 1/2, 1/3, and 1/4 filling, respectively. This power in the T dependence of $\rho_\parallel$ arises at or near commensurate fillings since dissipation along the chains is dominated by electron-electron umklapp scattering involving the nesting vector $2k_F$.

Transport perpendicular to the chains is prescribed by the theory for weakly coupled LLs,[21] with $\rho_\perp \propto T^{1-2\alpha}$. Here $\alpha=(K_c+1/K_c)/4-1/2$ is the anomalous exponent that governs the discontinuity of the electron occupation number at the Fermi surface.[20] As can be seen from the above expressions, LLs do not necessarily exhibit *metallic* resistivities with $d\rho/dT>0$. Also note that α depends quite sensitively on K_c, and thus a comparison of K_c and α determined from separate power-law fits to $\rho_\parallel$ and $\rho_\perp$, respectively, provides for a stringent self-consistency check on the analysis.

Photoemission experiments[5] indicate that the Fermi surface of $SrNbO_{3.41}$, is close to 1/3 filling, corresponding to $n_c=3$. For odd commensurability the $\rho_\parallel$ power-law exponent involves the parameter K_s which is not constrained by experiment. Nevertheless, we can demonstrate that a range of values for K_s exists for which K_c and α, determined from $\rho_\parallel$ and $\rho_\perp$ data, are in excellent agreement. A fit to the a axis data of Fig. 8 for the region[23] $T>80$ K yields $\beta=-1.05\pm0.05$, and thus $K_c=0.217\pm0.006-K_s/9$. A fit in the same T range[23] to the b axis data ($\rho_\perp$) yields $\alpha=0.90\pm0.04$. The latter value corresponds to $K_c=0.185\pm0.006$. These values of K_c agree for $K_s=0.29\pm0.1$.

The inferred values for $K_c(\simeq 0.2)$ are comparable to those determined for quasi-one-dimensional organic compounds,[24]

and imply relatively strong correlations. $K_s < 1$ implies spin-anisotropic interactions, as can arise from spin-orbit coupling or dipole-dipole interactions,[25] and a gap in the spin-excitation spectrum. The magnetic susceptibility χ of $SrNbO_{3.41}$ increases with temperature in the range of our fitting,[1,26] in a manner that is consistent with the presence of a spin gap.

Though the thermally activated resistivity behavior along the c axis seems inconsistent with the expression for $\rho_\perp$, it is important to emphasize that this expression arises in the theory for interchain transport[21] under the simplifying assumption that *no dissipation* (i.e., no umklapp scattering) occurs *along* the chains. This assumption is undoubtedly too crude to describe realistic systems. The incorporation of in-chain umklapps increases the tendency toward the opening of a Mott gap.[21] It is possible that the activation energy inferred for this transport direction is related to Mott localization but this issue remains open without further guidance from theory. Alternatively, the ρ_{cc} behavior might arise via thermal excitation to another conduction band near E_F. Band-structure calculations[5] indicate other bands near E_F but none with significant dispersion along the c axis.

IV. CONCLUSION

In conclusion, the diagonal components of the electrical resistivity tensor of $SrNbO_{3.41}$ have been determined using the Montgomery method. The results confirm quasi-1D behavior with a smaller anisotropy than previously reported. Linear thermal expansion reveals weakly anisotropic behavior that is atypical for low-dimensional oxides. The thermal expansion coefficients reveal no indications of an electronic phase transition, such as CDW formation. The heat capacity also does not reveal any features that might suggest the presence of a phase transition. The electronic heat-capacity coefficient is near zero, indicating localized electrons or a small density of states at the Fermi level. The weak anisotropy in the thermal expansion shows that the relative interatomic spacings remain fairly constant over the entire measurement range. This is significant since changes in relative interatomic spacing can drastically affect the physical properties of quasi-1D materials.[14] In this sense, $SrNbO_{3.41}$ may prove to be an important prototype compound for future investigation of quasi-1D behavior under nearly constant relative interatomic spacing over a broad temperature range.

Further analysis of the electrical resistivity reveals power-law behavior at $T \gtrsim 80$ K along the two most conducting crystallographic axes (a,b), with exponents consistent with Luttinger liquid theory and the experimental commensurability. This analysis implies strong correlations with Luttinger parameter $K_c \simeq 0.2$. The origin of the very small low-T energy gap remains a mystery, given that the apparently strong correlations inferred from the Luttinger liquid analysis tend to favor a large Mott gap. The activated behavior of the resistivity for $T \gtrsim 80$ K along the least conducting c axis is also a puzzle that may be associated with correlations or bands away from E_F.

ACKNOWLEDGMENTS

This material is based on work supported by the U.S. Department of Energy, Office of Basic Energy Sciences (Grant No. DE-FG-06ER46269), the National Science Foundation (Grants No. DMR-0504769 and No. DMR-0907036), an award from the Research Corporation, awards from CNPq (Grants No. 201.439/2007-7 and No. 301334/2007-2), and an award from FAPESP (Grant No. 2007/04572-8).

*Permanent address: Instituto de Ciências Tecnologia e Exatas, Universidade Federal do Triângulo Mineiro (UFTM), CEP 38025-180, Uberaba, MG, Brazil.

[1] F. Lichtenberg, A. Herrnberger, K. Wiedenmann, and J. Mannhart, Prog. Solid State Chem. **29**, 1 (2001).

[2] S. C. Abrahams, H. W. Schmalle, T. Williams, A. Reller, F. Lichtenberg, D. Widmer, J. G. Bednorz, R. Spreiter, Ch. Bosshard, and P. Günter, Acta Crystallogr., Sect. B: Struct. Sci. **54**, 399 (1998).

[3] The convention that the lowest electrical resistivity occurs along the a axis and the highest along the c axis is adopted in this work. As a result, the a and c axes are interchanged from the values reported in Ref. 2.

[4] C. A. Kuntscher, S. Schuppler, P. Haas, B. Gorshunov, M. Dressel, M. Grioni, F. Lichtenberg, A. Hernberger, F. Mayr, and J. Mannhart, Phys. Rev. Lett. **89**, 236403 (2002).

[5] C. A. Kuntscher, S. Gerhold, N. Nücker, T. R. Cummins, D.-H. Lu, S. Schuppler, C. S. Gopinath, F. Lichtenberg, J. Mannhart, and K. P. Bohnen, Phys. Rev. B **61**, 1876 (2000).

[6] H. Winter, S. Schuppler, and C. A. Kuntscher, J. Phys.: Condens. Matter **12**, 1735 (2000).

[7] H. C. Montgomery, J. Appl. Phys. **42**, 2971 (1971).

[8] B. F. Logan, S. O. Rice, and R. F. Wick, J. Appl. Phys. **42**, 2975 (1971).

[9] J. J. Neumeier, R. K. Bollinger, G. E. Timmins, C. R. Lane, R. D. Krogstad, and J. Macaluso, Rev. Sci. Instrum. **79**, 033903 (2008).

[10] J. W. Brill, M. Chung, Y.-K. Kuo, X. Zhan, E. Figueroa, and G. Mozurkewich, Phys. Rev. Lett. **74**, 1182 (1995).

[11] M. S. da Luz, A. de Campos, B. D. White, and J. J. Neumeier, Phys. Rev. B **79**, 233106 (2009).

[12] W. Kraus and G. Nolze, J. Appl. Crystallogr. **29**, 301 (1996).

[13] F. Lichtenberg, T. Williams, A. Reller, D. Widmer, and J. G. Bednorz, Z. Phys. B: Condens. Matter **84**, 369 (1991).

[14] C. A. M. dos Santos, B. D. White, Yu. Yi-Kuo, J. J. Neumeier, and J. A. Souza, Phys. Rev. Lett. **98**, 266405 (2007).

[15] H. Negishi, Y. Kuroiwa, H. Akamine, S. Aoyagi, A. Sawada, T. Shobu, S. Negishi, and M. Sasaki, Solid State Commun. **125**, 45 (2003).

[16] B. D. White, J. A. Souza, C. Chiorescu, J. J. Neumeier, and J. L. Cohn, Phys. Rev. B **79**, 104427 (2009).

[17] J. A. Souza, Y.-K. Yu, J. J. Neumeier, H. Terashita, and R. F. Jardim, Phys. Rev. Lett. **94**, 207209 (2005).

[18] C. Meingast, B. Blank, H. Bürkle, B. Obst, T. Wolf, H. Wühl, V.

Selvamanickam, and K. Salama, Phys. Rev. B **41**, 11299 (1990).
[19] F. R. Kroeger and C. A. Swenson, J. Appl. Phys. **48**, 853 (1977).
[20] J. Voit, Rep. Prog. Phys. **57**, 977 (1994); T. Giamarchi, Chem. Rev. **104**, 5037 (2004).
[21] A. Georges, T. Giamarchi, and N. Sandler, Phys. Rev. B **61**, 16393 (2000); A. Lopatin, A. Georges, and T. Giamarchi, *ibid.* **63**, 075109 (2001).
[22] A. Garg, D. Rasch, E. Shimshoni, and A. Rosch, Phys. Rev. Lett. **103**, 096402 (2009).
[23] A feature in the ρ_b data at 175 K (see Fig. 2) is propagated to the ρ_{aa} and ρ_{cc} data in the Montgomery analysis; this feature is an experimental artifact. In order to fit over the entire region $T > 80$ K, we fit the regions 80 K$\leq T \leq$175 K and 190 K$\leq T \leq$300 K, independently. The stated values of β and α are the averages from the two fits.
[24] M. Dressel, K. Petukhov, B. Salameh, P. Zornoza, and T. Giamarchi, Phys. Rev. B **71**, 075104 (2005).
[25] T. Giamarchi and H. J. Schulz, Phys. Rev. B **33**, 2066 (1986); J. Phys. (France) **49**, 819 (1988).
[26] J.-E. Weber, C. Kegler, N. Büttgen, H.-A. Krug von Nidda, A. Loidl, and F. Lichtenberg, Phys. Rev. B **64**, 235414 (2001).